Non-Local Model Analysis of Heat Pulse Propagation

Iwasaki, Takuya
Interdisciplinary Graduate School of Engineering Sciences, Kyushu University

Itoh, Sanae-I.
Research Institute for Applied Mechanics, Kyushu University

Yagi, Masatoshi
Research Institute for Applied Mechanics, Kyushu University

https://doi.org/10.5109/6786358

出版情報：Reports of Research Institute for Applied Mechanics. 44 (116), pp.87-106, 1998-10. 九州大学応用力学研究所

Non-Local Model Analysis of Heat Pulse Propagation

By Takuya IWASAKI*1, Sanae-I. ITOH*2 and Masatoshi YAGI*2

A new theoretical model equation which includes the non-local effect in the heat flux is proposed to study the transient transport phenomena. A non-local heat flux, which is expressed in terms of the integral equation, is superimposed on the conventional form of the heat flux. This model is applied to describe the experimental results from the power switching [Stroth U, et al 1996 *Plasma Phys. Control. Fusion* **38** 1087] and the power modulation experiments [Giannone L, et al 1992 *Nucl. Fusion* **32** 1985] in the W7-AS stellarator. A small fraction of non-local component in the heat flux is found to be very effective in modifying the response against an external modulation. The transient feature of the transport property, which are observed in the response of heat pulse propagation, are qualitatively reproduced by the transport simulations based on this model. A possibility is discussed to determine the correlation length of the non-local effect experimentally by use of the results of transport simulations.

Key Words: Transient transport, heat pulse propagation, non-local phenomena, plasma

1. Introduction

The anomalous transport in a high temperature plasma has been studied for a long time, from the beginning of the fusion research. Since the electron and ion heat channels in high temperature plasmas are clearly shown to be anomalous, it is of fundamental importance to investigate the heat diffusivity coefficient and to understand the physical mechanism causing the anomalous transport. The transport coefficient has been evaluated from the study of the heat pulse propagation after the sawtooth crash [1, 2]. It has been found that the heat diffusivity, χ_{HP}, derived by the heat pulse propagation is, in many cases, much larger than the heat diffusivity derived from the power balance analysis, χ_{PB}[2, 3]

Recently, the experimental data for the transient transport of heat pulse propagation in fusion plasmas has been accumulated [4, 5]. The characteristics of the transient transport, in comparison with the stationary state, have been studied in detail. It has been widely recognized that the effective heat diffusivity, i.e., the ratio between the heat flux and temperature gradient at the observation point, $r=r_{obs}$, seems to change much faster than the change of the local plasma parameter at $r=r_{obs}$. Such a fast change has also been observed in various circumstances of experiments. Fast inward propagation of the electron temperature perturbation caused by L-H transition and associated temperature increase in the central region has been observed on JET [6, 7, 8]. The temperature changes observed in the plasma core can occur on a much faster time scale than the time scale according to a diffusive propagation of the perturbation.

A systematic study of the transient transport problems has been reported on W7-AS. It was observed that the heat flux changes faster than the change of the temperature profile, responding to the switching of the central heating power [9]. A power modulation experiment using an electron cyclotron resonance heating (ECRH), which is localized at the center, has also been carried out [10]. In this experiment, it has been found that the value of electron heat diffusivity χ_e evaluated from heat pulse propaga-

*1 Interdisciplinary Graduate School of Engineering Sciences, Kyushu University

*2 Research Institute for Applied Mechanics, Kyushu University

tion is comparable to that calculated by the power balance. On the other hand, a new aspect is reported associated with the radial dependence of the phase delay. The delay time of the temperature modulation, compared to the center, is found to be a decreasing function of the radius in the outside of plasma. This implies that the electron temperature at the outside of plasma is affected faster than that at the half-radius by the central ECRH power modulation and can be considered as a sign of non-local transport [11].

The observation on the transient response has stimulated the transport modeling. The transport modeling relates the heat flux and the plasma parameters. There are some candidate-models which predict the power degradation of the energy confinement with the heating power. (1) An off-set linear model; $q=-n_e\chi_e\nabla T+q_{\mathrm{offset}}$ with χ_e and q_{offset} independent of ∇T and T. (2) Critical marginality [12] which implies the existence of a finite threshold in the temperature gradient, ∇T, for the excitation of the turbulence. (3) A non-linear χ_e model; $q=-n_e\chi_e\nabla T$ with $\chi_e\propto(\nabla T)^{\alpha}(T)^{\beta}$, where α and β are constant. (4) An empirical χ_e model, in which the thermal conductivity is assumed to depend on the heating power [9]; $q=-n_e\chi_e\nabla T$ with $\chi_e\propto\sqrt{P}$, where P is the heating power. Although all presented models predict the power degradation of the energy confinement, further development of the transport model is still necessary. The difference between χ_{PB} and χ_{HP}, i.e., non-linearity of χ_j (the subscript j represents the ion and electron), is discussed in chapter 2. The non-local nature of the heat flux is studied in this thesis. The first three models premise that a perturbation propagates as the result of diffusive process (i.e., the local flux changes only if the local gradient changes.). It means that the propagation of perturbation needs the transport time scale. Thus, the very fast transmission of a change in the diffusivity could not be reproduced by these models. These theoretical models are found to be insufficient to understand various transient transport [13, 14]. On the other hand, if the last model holds, then the rapid change of the heat diffusivity, which is caused by the change of heating at the different location, is naturally deduced. But it is difficult to derive, so far, such an expression from a theoretical point of view. The development of the transport modeling still remains to be an urgent problem.

In this thesis, we investigate a role of non-locality of plasma transport in the study of heat pulse propagation. For this purpose, a model equation is proposed, in which the non-local effect is taken into account in the heat flux. A non-local heat flux, which is expressed in terms of an integral equation, is superimposed on the conventional form of heat flux. A preliminary result has been reported that the non-local transport influences the transient transport [15]. The properties of this model are investigated by a transport simulation under the circumstances of other experiments in [9, 10]. It is shown that the gradient-flux relation has a hysteresis, when the heat flux is subject to the temporal variation. The heat flux can change faster than the change of the plasma parameter on a magnetic surface. This hysteresis nature disappears, if the change of source is slower than the typical energy confinement time. Under an oscillatory power input, the propagation of the oscillation across the plasma column is investigated. The radial dependence of the phase delay is calculated. It is shown that a small amount of non-local component is sufficient to make the phase delay be a decreasing function of radius near the plasma surface.

The organization of this paper is as follows: In Chapter 2, the transient response and non-local phenomena are briefly reviewed. In Chapter 3, the model equation is proposed and the properties of the model are explained. Using the model equation, the power switching experiment and power modulation experiment are simulated in Chapter 4. Summary and discussions are given in Chapter 5. Finally, a numerical algorithm for non-local model and its convergence check are presented in appendix.

2. Reviews

2.1 Transient Response

Perturbative transport studies are an elegant tool for investigating the parameter dependences of transport coefficients. The first experiments have been done with short microwave pulses in a spheromak [16] and on sawtooth propagation in the ORMAK tokamak [1]. Later, the technique has been extended to study particle and impurity transport. Most of the work, however, treats the electron thermal diffusivity as well as off diagonal elements of the transport matrix. A recent review of the vast experimental data which is now available can be found in Ref [4].

2.1.1 Heat pulse propagation induced by sawtooth crash

In this subsection, a method of measuring thermal diffusivity based on a heat pulse propagation induced by sawtooth crash is explained and is compared with that derived from power balance analysis. Let us start with the electron transport equation given by,

$$\frac{\partial}{\partial t}\left(\frac{3}{2}n_e T_e(r,t)\right)=\frac{1}{r}\frac{\partial}{\partial r}\left[r n_e \chi_e \frac{\partial T_e(r,t)}{\partial r}\right]+\Sigma Q, \tag{2.1}$$

where ΣQ represents all electron heat sources and sinks, such as Ohmic heating, collisional heat transfer to ions, convection, radiation and auxiliary heating. A small electron temperature perturbation induced by sawtooth crash $\widetilde{T}_e(r, t)$ is governed by the following equation

$$\frac{\partial}{\partial t}\left(\frac{3}{2}n_e \widetilde{T}_e(r,t)\right)=\frac{1}{r}\frac{\partial}{\partial r}\left[r n_e \chi_e \frac{\partial \widetilde{T}_e(r,t)}{\partial r}\right], \tag{2.2}$$

where we assume that the electron density n_e and diffusivity χ_e are constant in radius. This equation is derived by perturbing equation (2.1) and neglecting the source term because the equilibrium evolution implied by this term is slow and broadly distributed relative to the highly localized (in space and time) perturbation $\widetilde{T}_e(r, t)$. The initial condition is obtained from,

$$\widetilde{T}_e(r,0)=T_e(r,0)-T_{e0}(r), \tag{2.3}$$

where $T_{e0}(r)$ is the equilibrium temperature profile determined by

$$\frac{1}{r}\frac{\partial}{\partial r}\left[r n_e \chi_e \frac{\partial T_{e0}(r,t)}{\partial r}\right]+\Sigma Q=0. \tag{2.4}$$

The initial condition is shown in figure 2.1. Here r_0 is the radius to which reconnection (flattening of T_e) takes place and r_s is the singular surface $q=1$, where q is the safety factor. The relation $r_0 = \simeq\sqrt{2}r_s$ is hold. The schematic illustration of soft-X-ray diagnostic chords and the evolution of the electron temperature perturbation $\widetilde{T}_e(r, t)$ as a function of time are also shown in figure 2.1.

The signals below indicate the temporal variation of the soft-X-ray signals from the various chords (1-5). At later times $t_2>t_1>t_0$ the sawtooth induced heat pulse diffuses radially outwards from the radius r_0. For the initial profile of the electron temperature perturbation, we assume for simplicity that the initial perturbation can be described by the sum of an outer ($r=r_2$) positive delta function and an inner ($r=r_1$) negative delta function, where r_1 and r_2 are defined as $0<r_1<r_s$ and $r_s<r_2<r_0$, respectively. Using this initial condition, equation (2.2) can be solved. The result is as follows

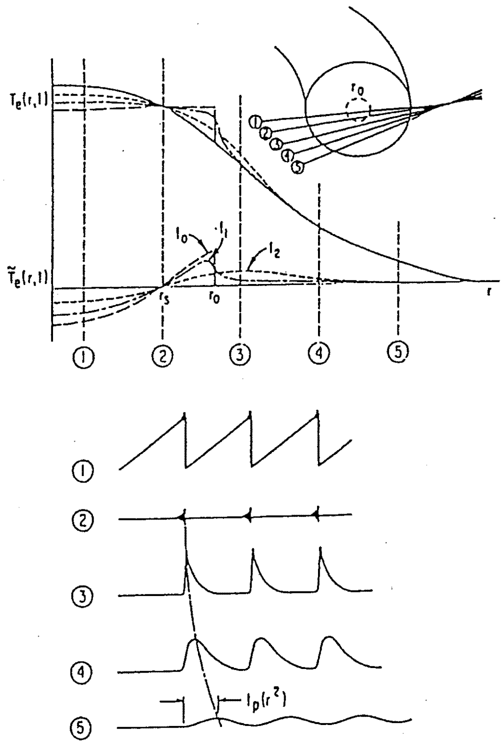

Fig. 2.1 Schematic illustration of soft-X-ray diagnostic chords and the evolution of the electron temperature perturbation $\widetilde{T}_e(r, t)$ as a function of time. The signals below indicate the temporal variation of the soft-X-ray signals from the various chords (1-5). At later times $t_2>t_1>t_0$ the sawtooth induced heat pulse diffuses outwards from the radius r_0 to which reconnection (flattening of T_e) takes place. (cited from Ref [2])

$$\tilde{T}_e(r,t) \sim \frac{r^2}{t^3}\exp\left(-\frac{3r^2}{8\chi_e t}\right). \tag{2.5}$$

Now a method for measuring χ_e based on observation of the time of arrival t_p of the peak of the heat pulses at different radii is explained using this result. t_p is estimated by the equation $\partial\tilde{T}_e/\partial t=0$ which gives the maximum value of $\tilde{T}_e$ for the time. Then we have the relation

$$\chi_e = \frac{r^2}{8t_p}. \tag{2.6}$$

If we plot the experimental time delay t_p of arrival of the heat pulse peak at different radii versus r^2, the observed slope should be a straight line giving directly χ_e for large values of r^2. This method obtaining χ_e-value is called simple time-to-peak method. A more complete discussion can be found in [17].

We define that χ_{HP} and χ_{PB} are thermal diffusivity derived by heat pulse propagation and that derived from power balance, respectively. χ_{HP} is evaluated by equation (2.6) and χ_{PB} is given by $\chi_{PB}=\int_0^r dr\Sigma Q/rn_e\frac{\partial Te}{\partial r}$. No good agreement is obtained between χ_{HP} and χ_{PB} if the analysis is done on the basis of a simple diffusive model [18]. The ratio of electron heat diffusivity χ_{HP} as measured by ECRH modulation or by sawtooth (sth) propagation to χ_{PB} as deduced from standard power balance analysis for various experiments are shown in Table 2.1 [19]. Usually, the relation

$$\frac{\chi_{HP}}{\chi_{PB}} > 1 \tag{2.7}$$

has been observed. Sometimes, however, the ratio is close to unity,

$$\frac{\chi_{HP}}{\chi_{PB}} \simeq 1 \tag{2.8}$$

It is a long-standing debate whether the difference between χ_{HP} and χ_{PB} is a genuine property of transport on an artifact introduced by the perturbation. It has been shown in the literature [20, 21] that χ_{HP} can significantly exceed χ_{PB} if χ_{PB} is an increasing function of ∇T_e and that such a dependence is consistent with global confinement properties. It has also been in the literature [22, 23] whether short-lived turbulence induced by the sawtooth instability itself could speed up the sawtooth heat pulse and thus corrupt the determination of χ_{HP}. This is normally referred to as "ballistic effect". A recent analysis of TFTR heat pulse date seems to indicate that the ballistic effect cannot be the sole cause for the observed large discrepancy between χ_{HP} and χ_{PB} [24].

2.1.2 Non-linearity of the heat flux on the temperature gradient

In this subsection, the discrepancy between χ_{HP} and χ_{PB} observed in experiments are explained based on non-linearity of the heat flux on the temperature gradient. The variation of the heat flux associated with the perturbation of the temperature is calculated from the various assumptions for the heat diffusivity. The dependence of the heat diffusivity on the temperature gradient is studied. The heat flux is expressed as

$$q_e = -n_e\chi_e(\nabla T_e)\nabla T_e. \tag{2.9}$$

The temperature, heat diffusivity and heat flux are linearized as follows

$$T_e = T_0 + \delta T, \tag{2.10}$$

$$\begin{aligned}\chi_e &= \chi_0 + \delta\chi \\ &= \chi_0 + \frac{d\chi_e(\nabla T)}{d\nabla T}\nabla\delta T,\end{aligned} \tag{2.11}$$

and

$$\begin{aligned}q_e &= q_0 + \delta q \\ &= -n_e\chi_e\nabla T_0 - n_e\left(\chi_0 + \frac{d\chi_e(\nabla T)}{d\nabla T}\nabla T_0\right)\nabla\delta T.\end{aligned} \tag{2.12}$$

Here we define χ_{PB} and χ_{HP} as

$$q_0 = -n_e\chi_{PB}\nabla T_0, \tag{2.13}$$

and

$$\delta q = -n_e\chi_{HP}\nabla\delta T, \tag{2.14}$$

respectively. From equations (2.12)-(2.14), we obtain

$$\chi_{PB} = \chi_0, \tag{2.15}$$

$$\chi_{HP} = \chi_0 + \frac{d\chi_e(\nabla T)}{d\nabla T}\nabla T_0. \tag{2.16}$$

In the case that the heat flux is a non-linear function of the temperature gradient, i.e., the power law

$$\chi_e \propto |\nabla T|^a \tag{2.17}$$

holds and χ_e is independent of T, equation (2.16) reduces to,

$$\chi_{HP} = (1+a)\chi_{PB} \tag{2.18}$$

Then the ratio of χ_{HP} to χ_{PB} is given as,

$$\frac{\chi_{HP}}{\chi_{PB}} = 1 + a > 1. \tag{2.19}$$

The power degradation of the energy confinement time

$$\tau_E \propto P_{\mathrm{heat}}^{-a/(1+a)} \tag{2.20}$$

is related to the non-linearity given in equation (2.17). If the power degradation takes place ($a>0$), the ratio χ_{HP}/χ_{PB} is larger than unity as is shown in equation (2.19).

Heat pulse propagation in tokamak plasma has been analyzed for various models which have the dependence of the temperature or temperature gradient [25]. The ratio (χ_{HP}/χ_{PB}) obtained from experiments shows more than 2. It has been shown that a model in which χ_e has a temperature gradient dependence could explain this ratio quantitatively. The simple diffusive models have not been able to explain the experimental observation on WT-3 tokamak. It has been also shown that the energy transport equation taking account of the convective term gives good fit to experimental result.

2.2 Non-local Phenomena

Recent observations in tokamaks and stellarators show that the non-local effect of transport is a key role in transient phenomena. Such transient phenomena explained in the following subsections have common nature that the local energy flux changes in the absence of a change in the thermodynamic variables. The change can be triggered from the plasma center or from the plasma edge, externally by the heating power, by impurity ablation or by pellets and intrinsically through low confinement mode (L mode) to high confinement mode (H mode) transitions.

2.2.1 L-H transition

The transition of a discharge from L to H mode confinement occurs on a time scale of 100μs. The initial confinement improvement is concentrated in a narrow edge region about 1cm wide. The subsequent increase in density and temperature can propagate

Table 2.1 Ratio of electron heat diffusivity χ_{HP} as measured by ECRH modulation or by sawtooth (sth) propagation to χ_{PB} as deduced from standard power balance analysis for various experiments. (cited from Ref [18])

Experiment	χ_e^{hp}/χ_e^{pb}	Reference	
ASDEX	3	(sth)	Giannone *et al* 1990
DIII-D	≈ 1	(ECRH)	Lopes Cardozo *et al* 1992b
DITE	≈ 1	(ECRH)	Hugill *et al* 1988
FTU	1.5-2.2	(sth)	Alladio *et al* 1992b
ISX-B	≈ 1	(sth)	Bell *et al* 1984
JET	2.5	(sth)	Tubbing *et al* 1987
JT-60U	2-4	(sth)	de Haas *et al* 1992
RTP	2-4	(sth)	Lopes Cardozo *et al* 1992a
RTP	2-4	(ECRH)	Lopes Cardozo *et al* 1992a
TEXT	2.25	(sth)	Brower *et al* 1990
TEXTOR	>4	(sth)	Krämer-Flecken, private communication
TFTR	$1->10$	(sth)	Fredrickson *et al* 1986
TORE SUPRA	2.5-3.5	(sth)	Lopes Cardozo *et al* 1992b
T10	≈ 1	(sth)	Sillen *et al* 1986
W7-AS	1-1.5	(ECHR)	Giannone *et al* 1991

radially inward and be analyzed in the spirit of a perturbative experiment. The temperature changes which are observed in the plasma core can occur, however, on a much faster time scale than that according to a diffusive propagation of the perturbation. This effect has been observed in low density discharges in JET [6]. In figure 2.2, an example from JET is shown [26]. The transition time is indicated by the sharp decay in the H_α trace. Already after a delay which is very short compared with the confinement time of ≈ 0.5s, the slope in the electron temperature evolution in the core responds to the change in the edge. Similar effects has been also observed in the ion energy and momentum transport channels [8]. The electron temperature evolution can be modeled best if the thermal electron diffusivity is changed everywhere from L to H mode level within ≈ 4ms [26]. It is difficult to explain the experimental result based on a local model, unless a highly complicated non-linear dependence of the heat diffusivity on the temperature or temperature gradient is assumed.

Radial mode coupling of turbulence is suggested as a possible process to explain the fast communication of the edge with the core plasma. Confirmation for this approach is found in a fast response of the density fluctuation amplitude [26].

2.2.2 Cold pulse propagation

Impurity injection into the plasma edge has been proposed as an alternative method to generate perturbations in the electron temperature for transient transport studies. Results from first experiments in TFTR [27] are similar to those from heat pulse propagation experiments. The cold pulse propagation is consistent with a diffusivity which is four times larger than the power balance value.

Experiments in the TEXT tokamak [28], also in JET [29], have reveled, however, the importance of non-local effects in the response of transport to impurity injection. Figure 2.3 shows a very clear violation of local transport in TEXT [28]. Carbon has been introduced by the laser ablation technique in order to cool the plasma edge. The radiation is limited to the outer 10% of the plasma radius. The produced cold pulse propagates diffusively inward. It is noted that the temperature in the plasma core rises, although it drops in the peripheral region by the trigger. The temporal evolution can be modeled if the

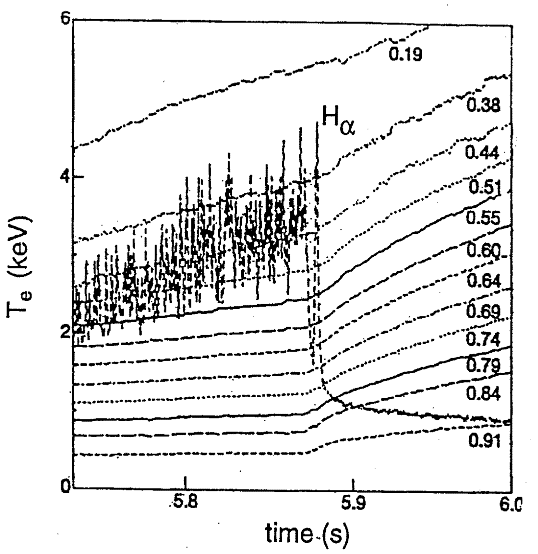

Fig. 2.2 Electron temperature versus time for different radii during an L to H transition in JET. The superposed H_α signal indicates the time point of the transition. The normalized radii of the temperature measurements are given on the right. (cited from Ref [24])

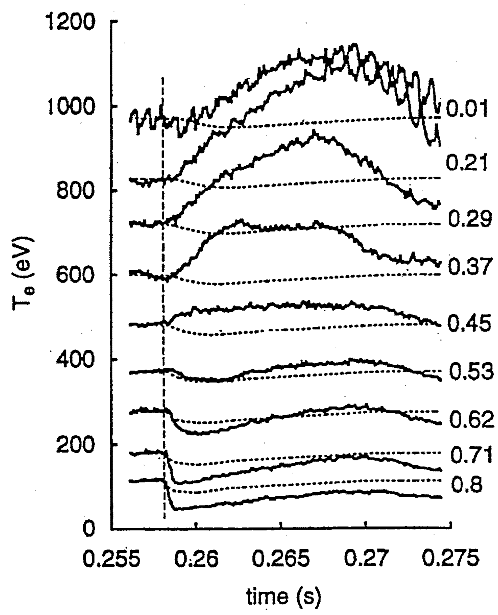

Fig. 2.3 Electron temperature evolution at different radii (indicated on the right) after carbon impurity injection in the plasma edge of TEXT. The dashed lines correspond to diffusion based on a local transport model. (cited from Ref [26])

thermal diffusivity increases by a factor of three to four in the outer 25% of the plasma radius on a time scale of about 100μs and everywhere else by a factor of 2 in less than 1ms. Since the ohmic heating power cannot change on this time scale, the reduction in the diffusivity generates an increasing temperature in the core.

2.2.3 Power switching experiment on W7-AS

The signature of non-local transport phenomena in the previous experiments has shown a fast response of the electron temperature. On the other hand, in experiments with power steps in W7-AS, the non-local transport has been concluded from too slow response of the temperature [11]. After the switch on-off of the centrally absorbed ECRH power, the temporal evolution of the electron temperature profile is analyzed by means of a power balance. The slowing-down time of the non-thermal electron population produced by ECRH is shorter than 0.1ms. Hence, changes in power occur almost instantaneously.

Figure 2.4 shows the diffusivity from a power balance analysis outside the deposition zone. The response to power step from 0.2 to 0.65MW is instantaneous and decoupled from the temperature evolution. Right after changes in the power, the diffusivity jumps to the value, which corresponds to the new power level.

The analysis of the dynamic phases needs an important input of the radial power deposition profile. A mechanism which could make the power deposition profile broader than expected from theory is related to suprathermal electrons produced by ECRH. Due to the gradient in the magnetic field, particles which are trapped in a helical magnetic mirror suffer vertical drifts leading to radial displacements and power deposition outside the central heating location. In order to investigate this effect, experiments have been carried out in a configuration with a local magnetic field maximum at the heating location to be compared with the standard configuration, which has a small magnetic mirror.

A time-dependent simulation code was used to model the dynamic phases of the experiments in the two configurations [30]. In figure 2.5, the ECE electron temperature drop for the phase after the power was decreased is compared with simulations using the power, temperature and temperature gradient dependent model of $\chi(r)\sim P^{0.5}$ (solid line), $\chi(r)\sim T(r)$ (dashed line) and $\chi(r)\sim\nabla T(r)$ (dotted line). Only the global model satisfactorily describes the evolution of the temperature. All local models predict a much faster evolution of the temperature than that measured.

The temporal evolution in both magnetic configurations is similar. In the magnetic-hill configuration

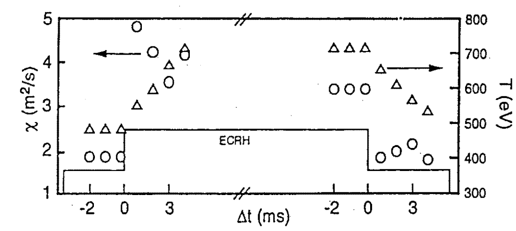

Fig. 2.4 Time evolution of the radially averaged ($0.35\leq r/a\leq 0.85$) electron thermal diffusivity and temperature during the dynamic phases after changes in heating power. (cited from Ref[9])

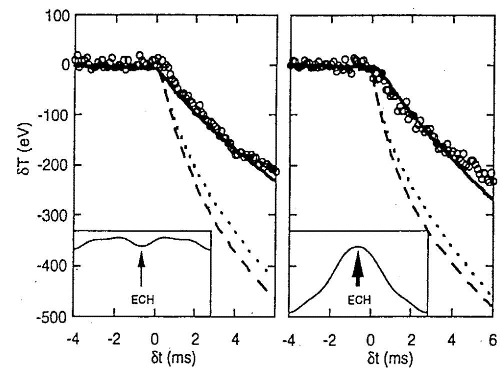

Fig. 2.5 Simulations of the dynamic phase after decreasing the ECH power at $\delta t=0$ by 0.45MW. Three models are used: $\chi(r)\sim P^{0.5}$ (solid line), $\chi(r)\sim T(r)$ (dashed line) and $\chi(r)\sim\nabla T(r)$ (dotted line). The simulated changes in T are compared with ECE date at $r/a=0.22$. The experiments were carried out in the standard magnetic configuration (left) and a hill configuration (right), where the ECH is absorbed in a local minimum and maximum of the magnetic field, respectively (see inserts). (cited from Ref [9])

there are no trapped particles to be heated. Hence, an appreciable modification of the power deposition profile due to trapped particles can also be ruled out in the standard configuration.

Together with the observed power degradation, these results can be interpreted in terms of the global model, which is illustrated in figure 2.6. If χ is a function of ∇T, the energy flux is given by the solid line. χ corresponds to the slope of a line from the origin to the respective point on the line. By modulation the power by δP the slope of a tangent is measured as transport coefficient χ^{inc} [31], being larger than χ from the power balance. If χ changes, however, on a short timescale with P, the local heat flux q follows the broad arrows: starting from position (1), q decreases at constant ∇T when the power is decreased until the slope corresponds to χ^- valid for steady state. q runs through the second half of the hysteresis when the power is increased again. The result is a heat pulse which propagates not with χ^{inc} but with an average value of χ^- and χ^+, both being very close to the value measured by the power balance.

2.2.4 Power modulation experiment on W7-AS

The power modulation experiments have been carried out on the W7-AS [10]. The deposition of

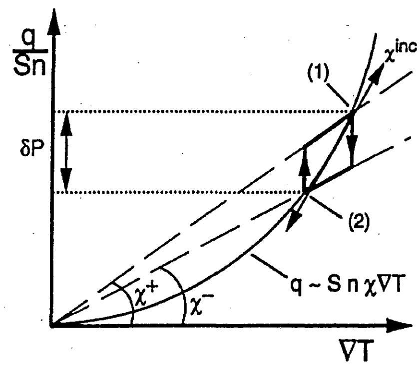

Fig. 2.6 Anomalous electron heat transport according to models which depend nonlinearly on the temperature gradient (solid and dashed lines) and the hysteresis which describes the plasma in a heat pulse cycle according to a global model (indicated by arrows). (cited from Ref [9])

ECRH power is highly localized in the plasma center, so that the power modulation produces heat pulses which propagate away from the deposition volume. Radiometry of the electron cyclotron emission is used to measure the generated temperature perturbation. The propagation time delay of the temperature perturbation as a function of distance to the power deposition region is used to determine the electron thermal duffusivity. This value is compared with the value determined by global power balance. In contrast to sawtooth propagation experiments in tokamak, it is found that the value of χ_e from the heat pulse propagation is comparable to that calculated by the power balance.

For on-axis modulation in the high density discharge, a typical result of the radial dependence of the predicted and measured time delay on the inside (high field side) and outside (low field side) of the plasma column at the modulation frequency f_M=46Hz and 276Hz is shown in figure 2.7. It can be seen that the good agreement of the time delay measurements from the inside and outside of the plasma is found only in the vicinity of the plasma center. From these results, a new aspect is reported associated with the radial dependence of the phase delay. The delay time of the temperature modulation, compared to the center, is found to be a decreasing function of the radius in the outside of plasma. This implies that the electron temperature at the outside of plasma is affected faster than that at the half-radius by the central ECRH power modulation and can be considered as a sign of non-local transport [11].

3. Non-local Transport Model

In this section, we present our theoretical model and explain its properties. To investigate the transient response of the electron temperature, let us start with the transport equation for the electron temperature

$$\frac{\partial}{\partial t}\left(\frac{3}{2}n_e T(r,t)\right) = -\nabla \cdot q(r,t) + \Sigma Q, \qquad (3.1)$$

where n_e, $T(r, t)$, $q(r, t)$ and ΣQ represent the electron density, temperature, heat flux and sources/sinks, respectively. The boundary conditions are set to be $q(0, t)=0$ and $T(a, t)=0$, where a is the plasma minor radius. For simplicity,we use a constant density approximation in the model calculations.

To take the non-local effect and the non-Markovian process in the heat flux into account, the heat flux is modeled as

$$q(r,t)=-\int_{-\infty}^{t} dt' H(t-t')\int_{0}^{a} dr' K_l(r-r') \times n_e \chi_e (T(r',t'), \nabla T(r',t')) \nabla T(r',t'), \tag{3.2}$$

where χ_e is the (generalized) electron heat diffusivity which is generally a function of the temperature or temperature gradient and $K_l(r-r')$ and $H(t-t')$ are the kernels which include the non-local effect and the non-Markovian process. It is possible that the plasma is affected by the memory of the past plasma state. Although equation (3.2) is a general expression for the heat flux, we, in this article, concentrate on the model that the transport is governed by the Markovian process and choose $H(t-t')=\delta(t-t')$, where $\delta(t-t')$ is a delta function.

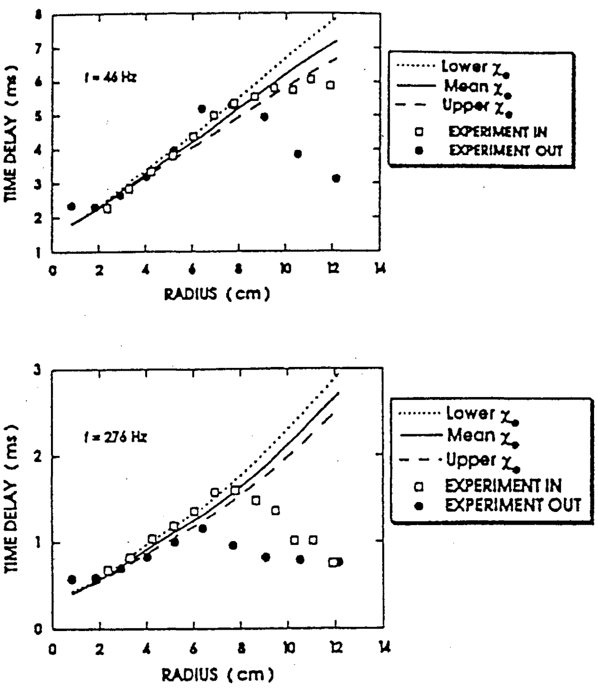

Fig. 2.7 Predicted and measured time delay in the high density discharge at f_M=46Hz and f_M=276Hz from the inside (hollow symbol) and outside (full symbol) of the plasma column, assuming $\chi_e=1.1\pm 0.2\chi_{PB}$. (cited from Ref [10])

Then, the heat flux is reduced to as follows

$$q(r,t)=-\int_{0}^{a} dr' K_l(r-r') \times n_e \chi_e (T(r',t), \nabla T(r',t)) \nabla T(r',t). \tag{3.3}$$

This expression suggests that the heat flux at r is influenced by the temperature and its gradient far from the location r. If the relation like equation (3.3) holds, then a very fast change of the heat flux is possible. The heat flux at r changes when the plasma parameter at r' is modified, without the change of plasma parameters at r.

Equation (3.3) has the following physical meaning. Suppose that the anomalous transport is caused by some fluctuations, whose property at r is determined by the plasma structure within the radial correlation lengths. Then temperature and temperature gradient at r' could be influential on the fluctuating plasma parameter at r, if the distance $|r-r'|$ is shorter than the correlation length. Thus the heat flux at r could depend on the parameter at r'.

In this study, we choose the following expression for the kernel

$$K_l(r-r') \equiv \frac{r}{r'} \times \left\{ C_{\mathrm{local}} \delta(r-r') + C_{\mathrm{global}} \frac{1}{\sqrt{\pi}\, l} \exp\left[-\left(\frac{r-r'}{l} \right)^2 \right] \right\}, \tag{3.4}$$

where C_{local} and C_{global} are the numerical constants which represent the local effect and the non-local effect, l is the half width where the non-local effect appears and $\delta(r-r')$ is a delta function. The constraint for the numerical constants is imposed to be $C_{\mathrm{local}} + C_{\mathrm{global}} = 1$. The weighting function r/r' is introduced to give the boundary condition, $q(0, t)=0$. The second term in the right hand side becomes the delta function when $l \to 0$. In this limit (or when $C_{\mathrm{global}}=0$ holds), the heat flux is reduced to the one of the local transport model. Namely, when the kernel is set to be the delta function, then the heat flux is given by $q(r)=-n_e \chi_e \nabla T(r)$.

The form (3.4) shows that we take two classes of fluctuations, i.e., the microscopic fluctuations with a very short radial correlation length and the one with a long correlation length. The plasma turbulence due to non-linear excitation [32] could generate very long correlated structures across the magnetic field. The discussion for the non-linear theory is out of the scope of this thesis. We here only notice that the experimental study has suggested the existence of a non-local heat flux component which has the nature of the Bohm-type diffusion [33]. It has been pointed out that such a dependence of the thermal diffusivity is related to the long-wavelength mode according to the theory of scale-invariance [34].

Substituting equations (3.3) and (3.4) into equation (3.1), we obtain

$$\frac{3}{2}\frac{\partial T(r,t)}{\partial t}$$
$$=C_{\text{local}}\frac{1}{r}\frac{\partial}{\partial r}\left(r\chi_e(T(r,t),\nabla T(r,))\frac{\partial T(r,t)}{\partial r}\right)$$
$$+C_{\text{global}}\frac{1}{r}\frac{\partial}{\partial r}\left\{r\int_0^a dr'\frac{1}{\sqrt{\pi}\,l}\exp\left[-\left(\frac{r-r'}{l}\right)^2\right]\right.$$
$$\left.\times\frac{r}{r'}\chi_e(T(r',t),\nabla T(r',t))\frac{\partial T(r',t)}{\partial r'}\right\}+\frac{\Sigma Q}{n_e}. \tag{3.5}$$

The energy transport equation is re-formulated into an integro-differential equation from the differential equation used in a local transport model.

The power deposition profile in this study is modeled as

$$P(r,t)=P_0(t)\exp\left[-A^2\left(\frac{r}{a}\right)^2\right], \tag{3.6}$$

where $A>0$ and the power is mainly deposited in the region, $r/a\leq 1/A$. The schematic drawings of the temperature profile, the kernel profile and the power deposition profile ($A=10$) are shown in figure 3.1, where the horizontal axis is taken as the normalized plasma radius. Throughout the thesis we take $A=10$ unless specified. The heat flux at r is determined by the temperature gradient weighted by the kernel. The heat flux at the location away from the heat deposition (e.g., $r/a=0.3$) is shown to be strongly influenced by the temperature profile in the heated region.

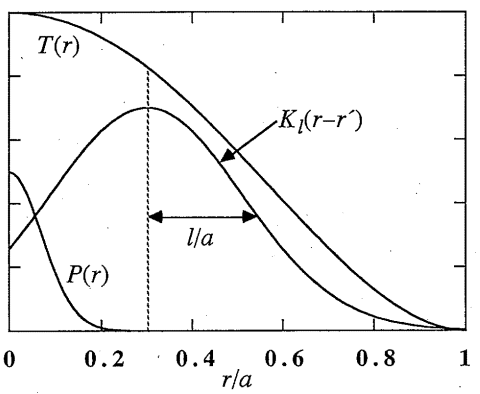

Fig. 3.1 The profiles of $T(r)$, $K_l(r-r')$ and $P(r)$. $l/a=0.3$ and $A=10$ are assumed. Transient response is observed at $r/a=0.3$.

4. Application of the Non-local Transport Model

4.1 Analyses for the power switching experiment

The energy transport equation, i.e., equation (3.5), is solved under the condition given in the previous section and the time evolution of the temperature profile is analyzed. As a first example, the electron density and heat diffusivity are assumed to be constant. The possible difference in transport coefficients against the perturbation, which is caused by the non-linear dependence of the transport coefficient on the gradient [4, 25], is eliminated. This simplification in χ_e allows us to concentrate on the role of the non-local transport in the transient response.

The assumed temporal evolution of the central heating power is shown is figure 4.1 which simulates

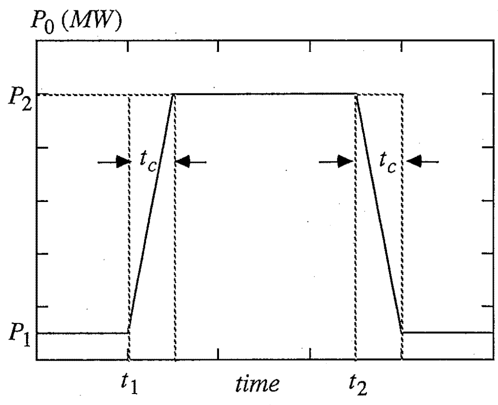

Fig. 4.1 The assumed temporal evolution of the heating power. The heating power changes from 0.1MW to 1.0MW. The change of the heating power takes place with the time interval of t_c.

the experiment [9]. The heating power changes from P_1 to P_2 with the rise time of t_c. Since the nature of the transient response is attributed to the fast change of the plasma state, the limit of $t_c \rightarrow 0$ is analyzed when we investigate the transient response. On the other hand, when $t_c \rightarrow \infty$, the change takes place as a continual change between the stationary profiles. We first set $t_c=0$ to elucidate the non-local effect and study the dependence on t_c later. We use the following plasma parameters for the simulation study of experiments in W7-AS reviewed in subsection 2.2.3 and 2.2.4 (The heat deposition profile is as in equation (3.6) with $A=10$). Major and minor radii are $R=2.0$m and $a=0.2$m, respectively. The constant electron density and diffusivity are chosen as $n_e=4.0\times10^{19}\mathrm{m}^{-3}$ and $\chi_e=1.0\mathrm{m}^2/\mathrm{sec}$. Then energy confinement time becomes $\tau_E \approx a^2/2\chi_e=20$ ms. The value of numerical constants $C_{local}=0.9$ and $C_{global}=0.1$ are chosen unless specified. The levels of input power are chosen as $P_1=0.1$MW and $P_2=1.0$ MW, respectively.

Equation (3.5) is solved and the transient response of the temperature profile is analyzed. Figure 4.2 (a) illustrates the dynamic relation between the temperature gradient and the heat flux which are to be observed at the radius, $r/a=0.5$, where parameters $l/a=0.5$ and $C_{global}=0.1$ are used. The vertical axis is the heat flux and the horizontal axis corresponds to the temperature gradient. When the heating power is increased at $t=t_1$ (with $t_c=0$), the heat flux starts to increase faster than the temperature gradient does. With a finite delay time, the temperature gradient starts to rise. Then the dynamic relation follows the line indicated by the arrow. On the other hand, when the power is suddenly dropped at $t=t_2$, the heat flux reduces faster than the temperature gradient does. A hysteresis curve is obtained in the gradient-flux relation and the dynamics follows on the curve in the clockwise direction. The observation point $r/a=0.5$ in figure 4.2 (a) is away from the region of heat deposition. An essence of the transient response, i.e., the hysteresis in the gradient-flux relation,is reproduced by the non-local transport model. In a local model, the heat flux is proportional to the temperature gradient if the electron density and diffusivity are constant. A straight line is obtained as is also shown by the dashed line in figure 4.2 (a) for $C_{local}=1$ and $C_{global}=0$. It is noted that the hysteresis cannot be obtained even in the non-linear model, i.e., $\chi_e \propto |\nabla T|^{\alpha}$. In figure 4.2 (b), the transient responses observed at $r/a=0.1$ and $r/a=0.3$ are shown in addition to that at $r/a=0.5$. The position $r/a=0.1$ is located in the region which is heated directly, there the parameters are found to follow on the hysteresis curve (thin) in the counter-clockwise direction.

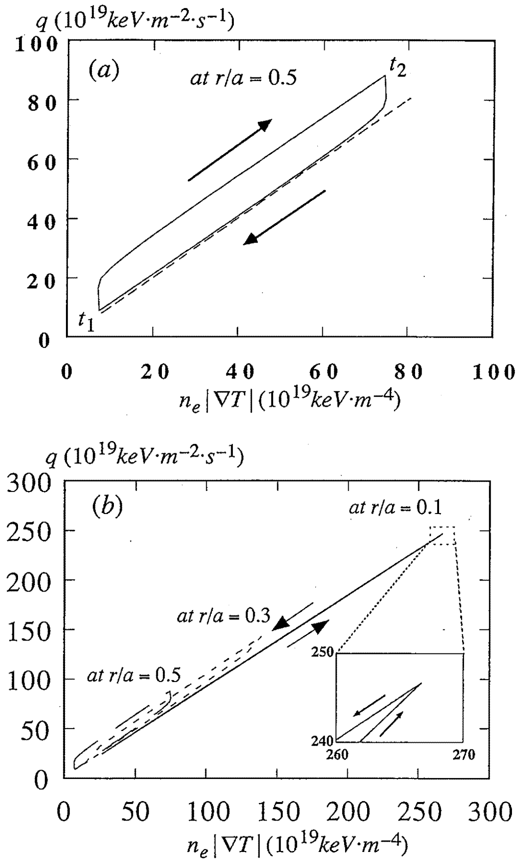

Fig. 4.2 The dynamic gradient-flux relation as the transient response. The hysteresis is observed at $r/a=0.5$, the location of which is away from the power deposition region (a). The discharge follows on the hysteresis line in a clockwise manner. When $l/a=0$, the hysteresis disappears (dashed line). The hysteresis is observed at $r/a=0.1$, $r/a=0.3$ and $r/a=0.5$ (b). At $r/a=0.1$ the temporal change in the relation follows the hysteresis in a counter-clockwise way. (The magnified figure is also drawn on the lower right side.) Parameters are set $A=10$, $l/a=0.5$ and $C_{global}=0.1$.

The difference between the directions in the response can be understood as follows: The heat flux at the location $r/a=0.5$ is affected directly by the rapid change of central temperature through the non-local effect when the additional power is switched on, but the temperature at $r/a=0.5$ is indirectly affected by the non-local effect so that its change is slow. On the other hand, in the region which is heated directly, the temperature gradient increases rapidly but the heat flux increases slowly when the additional power is switched on, because the heat flux depends also on plasma parameters away from the directly heated region. The hysteresis becomes counter-clockwise in this case. The points of the hysteresis corresponding to the stationary phases, which are the upper right point and the lower left point of the hysteresis, are not on the line for the local model shown by the dashed line. This is because the steady state temperature profile with the non-local effect is slightly different from that in the local transport model.

Next we examine the width of the hysteresis. The width of the hysteresis is defined as the ratio of a minor axis to a major axis of the gradient-flux curve by the analogy to a conic section. The width at the observation point r/a is plotted in figure 4.3 for various values of correlation length l/a, i.e., $l/a=0.3$, $l/a=0.5$, $l/a=0.7$ and $l/a=0.9$, where we set $C_{\mathrm{global}}=0.1$. The horizontal axis is the normalized plasma radius. At a particular radius $r=r_0$ (≈ 0.15), the width of the hysteresis vanishes. The half width of the central heating ($A=10$) is comparable to this value. The region $r<r_0$ is heated directly and the hysteresis is counter-clockwise. The hysteresis is clockwise for $r>r_0$. Curves drawn in figure 4.3 have the peak values at $r/a \approx l/a+r_0$ ($\chi_e=const$ case for $r>r_0$). This fact indicates that if the width of the hysteresis is plotted at various position and if the peak value is found in an experiment, an estimate of the correlation length may be done from figure 4.3.

We examine the effect of a finite switching time t_c. It is expected that the non-locality, i.e., the hysteresis nature, becomes less noticeable with the increase of t_c. The dependence of the width of the hysteresis on t_c is shown in figure 4.4, where the vertical axis is the width of the hysteresis and the horizontal axis is the switching time of the central heating power, t_c, normalized to the energy confinement time, τ_E. The parameters $l/a=0.5$ and $C_{\mathrm{global}}=0.1$ are chosen. We can see from figure 4.4 that the width has the maximum value at $t_c=0$ and monotonically decreases with the increase of t_c, which behaves as $1/t_c$ for the limit $t_c/\tau_E \gg 1$. In the limit $t_c \to \infty$, the width vanishes, which corresponds to the stationary case. The hysteresis is prominent when $t_c \ll \tau_E$.

4.2 Analyses for the power modulation experiment

In this section, the power modulation experi-

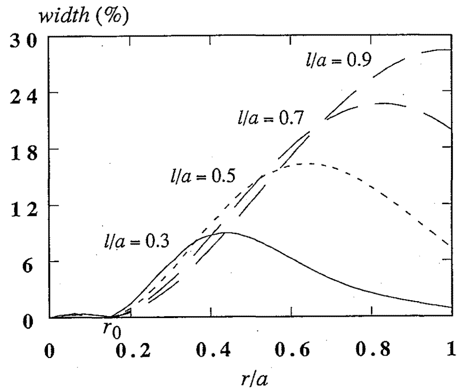

Fig. 4.3 The width of the hysteresis is plotted against the observed point for $l/a=0.3$, 0.5, 0.7 and 0.9, where we set $C_{\mathrm{global}}=0.1$. r_0 is the position where the width vanishes. These curves have the peak values at $r/a \approx l/a+r_0$.

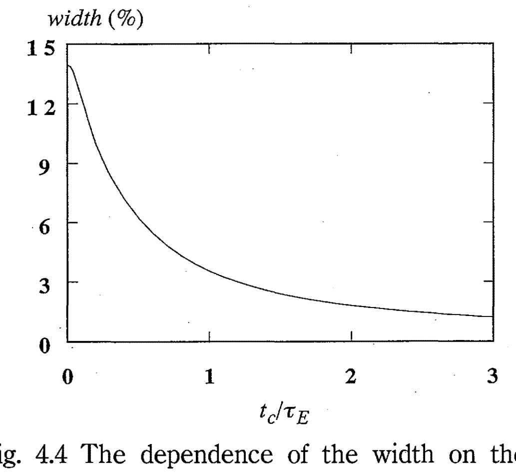

Fig. 4.4 The dependence of the width on the switching time t_c. The parameters $l/a=0.5$ and $C_{\mathrm{global}}=0.1$ are chosen. The width monotonically decreases with t_c.

ment is simulated to study the response of the plasma temperature perturbation. The heating power, which is centrally localized as is modeled by equation (3.6), is modulated in time with the frequency f_M as is shown in figure 4.5. The heating power is switched between $P_0=0.5$ and $P_0=0.35$MW. The duty cycle is 2/3, i.e., the ratio of the time interval at maximum power to the time interval of a cycle. In W7-AS experiments, a duty cycle of 2/3 is chosen instead of 1/2. This is because a larger Fourier amplitude at the second harmonics of the modulation frequency is obtained in the case with duty cycle 2/3 [35]. When the modulation period far exceeds the energy confinement time, which is approximately 20 ms in this case, the change of the temperature takes place as a continual change between the stationary profiles, therefore little new information would be obtained. Thus the constraint must be imposed as

$$2\pi f_M \tau_E > 1. \tag{4.1}$$

This implies that the modulation frequency must be larger than 10Hz in this case. The boundary conditions are set to be $q(0,t)=0$ and $T(a,t)=0$, if not specified.

Responding to the power modulation, there appears a modulation of the temperature. The perturbation of the temperature, $\delta T(r,t)$, is Fourier-decomposed as

$$\delta T(r,t)=\sum_{k=0}^{\infty} a_k(r)\cos(2\pi k f_M t-\varphi_k(r)), \tag{4.2}$$

where $a_k(r)$ and $\varphi_k(r)$ are the amplitude and phase

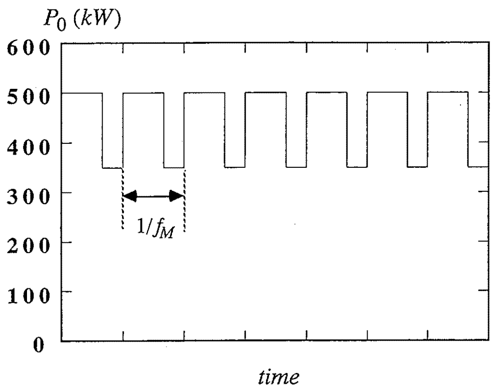

Fig. 4.5 The assumed temporal evolution of the heating power. The power is modulated from 350kW to 500kW with the period, $1/f_M$.

of k-th harmonics at r. The phase difference is defined as

$$\Delta\varphi_k(r)=\varphi_k(r)-\varphi_k(0), \tag{4.3}$$

which corresponds to the time delay of the pulse.

The results of the radial dependence of the amplitude and phase difference confirm the results obtained with a simple power-dependent model [11]. Typical results are shown in figure 4.6 for the fundamental frequency. In this case, the parameters f_M=30Hz and $C_{global}=0.1$ are chosen. The dotted line and solid line correspond to the cases with $l/a=0.36$ and $l/a=0.5$. The dashed line is plotted as the

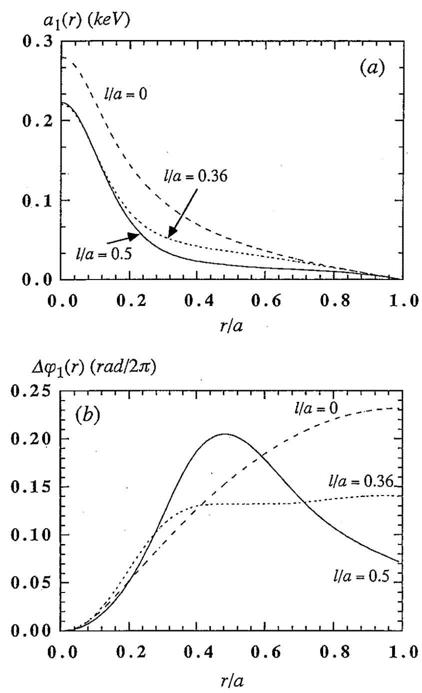

Fig. 4.6 The radial dependence of the perturbed temperature amplitude (a) and the radial dependence of the phase difference in the temperature perturbations (b). The fundamental component is shown. The solid, dotted and dashed lines are obtained for the cases of $l/a=0.5$, 0.36 and 0, respectively. We set $C_{global}=0.1$ and f_M=30Hz. If the non-local effect is taken into account, the magnitude of the amplitude is reduced. In a local transport model, the phase difference increases monotonically with the increase of the radius. For $l/a=0.5$, the reversed phase appears.

reference case with $l/a=0$ (or equivalently $C_{\mathrm{global}}=0$), i.e., the local transport model. From figure 4.6(a), it is found that if the non-local effect is taken into account, the magnitude of the amplitude is reduced. The suppression of the amplitude increases at larger radii. At larger f_{M}, this tendency is more pronounced and at larger plasma radii the amplitude becomes so small, that the numerical accuracy cannot be ensured. Thus frequencies smaller than 100Hz are used in this paper. It is found that the radial shape of the amplitude $a_k(r)$ depends, only quantitatively, on the parameters f_{M}, C_{global} and l/a. A qualitative difference is not seen in $a_k(r)$. On the contrary, the phase difference $\Delta\varphi_k(r)$ is found to show a qualitative change depending on the paramenters f_{M} and C_{global} and l/a. The radial dependence of the phase difference is investigated. In the local transport model, the phase difference monotonically increases with radius, so that the pulse propagates from the inside to the outside gradually (dashed line in figure 4.6(b)). On the other hand, it is found that when l/a increases, the phase difference becomes flat in the outside region (the case of $l/a=0.36$ denoted by the dotted line in figure 4.6(b)) and then it becomes a non-monotonic function of the radius which is reversed at outside (the case of $l/a=0.5$ denoted by the solid line in figure 4.6 (b)). In the case of $l/a=0.5$, the curve has the peak value at $r/a=0.48$. It seems as if the signal propagates from the edge, although the perturbation is actually excited at the center. Or it seems that the plasma in the outside region is affected by the central power modulation faster than the plasma in the middle region is. The reversed phase is obtained in this simulation which may correspond to the finding of the experiment in W7-AS.

A fixed boundary temperature is imposed at the edge as a boundary condition, i.e., $T(a)=0$. Thus there is a possibility that the reversed phase appears not due to a non-locality but due to a reflection of the pulse at the boundary. To investigate the boundary effect, we test following two cases. At first, the boundary condition is changed from $T(a)=0$ to $d\ln T(r)/dr=const$ at $r=a$, i.e., from the fixed boundary condition to the free boundary condition. The cases with different boundary conditions are compared in figure 4.7. In this figure, parameters $f_{\mathrm{M}}=30$Hz, $C_{\mathrm{global}}=0.1$ and $l/a=0.5$ are chosen. Any substantial change of the radial dependence of the phase difference is not observed even if the free boundary condition is imposed. Next, we clarify the impact of the non-local term by cutting off the integral in the outside region. We integrate equation (3.5) over r from 0 to εa instead of from 0 to a, where ε is chosen between 0 and 1. Then the integral of the second term is right hand side of equation (3.5) is replaced as $\int_0^a dr'$

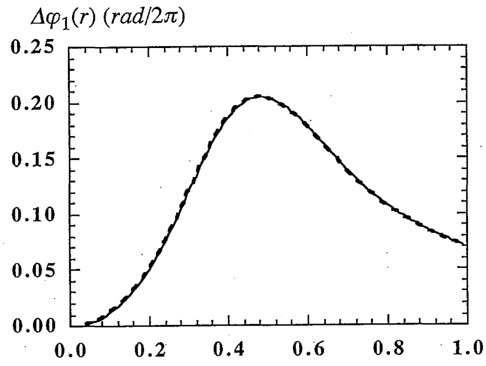

Fig. 4.7 The radial profiles of the phase difference with different boundary conditions. The solid and dashed lines are obtained for the fixed and free boundary conditions, respectively. We set $C_{\mathrm{global}}=0.1$, $f_{\mathrm{M}}=30$Hz and $l/a=0.5$.

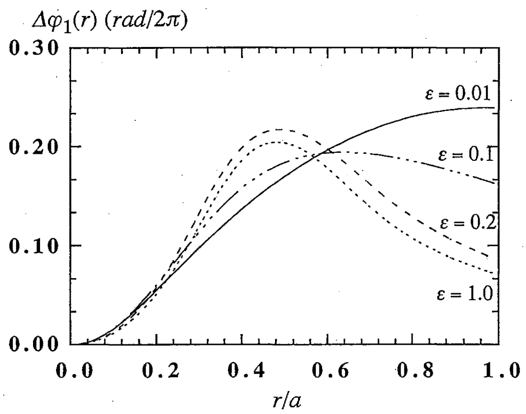

Fig. 4.8 The radial profiles of the phase difference for an artificial change in integration region. The solid, triple dotted dashed, dashed and dotted lines are obtained for $\varepsilon=0.01$, 0.1, 0.2 and 1.0, respectively. We set $C_{\mathrm{global}}=0.1$, $f_{\mathrm{M}}=30$ Hz and $l/a=0.5$. Even when $\varepsilon=0.2$, the reversed phase clearly appears.

$\rightarrow \int_0^{\varepsilon a} dr'$. If ε is 0, then the non-local effect vanishes and if ε is 1, the non-local effect is taken into account in the whole region. The result is shown in figure 4.8, where f_M=30Hz, C_{global}=0.1 and l/a=0.5 are chosen. Then solid line, triple dotted dashed line, dashed line and dotted line are obtained for ε=0.01, 0.1, 0.2 and 1.0, respectively. It can be seen from figure 4.8 that the reversed phase appears clearly even when ε is 0.2. Even if the value of ε is changed from 0.2 to 1.0, a qualitative change in the radial dependence of phase difference cannot be seen. When ε=0.01, which is almost 0, the phase difference increases with the radius and the reversed phase disappears as is expected. For the second harmonics, the similar result is obtained. Therefore it is concluded that the appearance of reversed phase is not related to the sort of the boundary condition such as the reflection of the pulse at the boundary. The reversal of the phase delay $\Delta\varphi_k(r)$ is caused by the interaction with the core-region through the non-local effect itself.

Next, we examine the position where the phase begins to reverse.

Frequency dependence

The dependence of phase reversed position on the frequency is shown if figure 4.9 for various values of non-local parameter, l/a=0.4 (□) and l/a=0.5 (◇), where C_{global} is fixed to 0.1. The vertical axis is the radial position where the phase is reversed and the horizontal axis is the frequency. The reversed phase is not seen in the case with l/a=0.3. On the other hand the reversed phase is clearly observed in the case with l/a=0.4 and l/a=0.5. The critical value of l/a for the appearance of the reversed phase is found in between l/a=0.3 and l/a=0.4 and above the critical value, it is not sensitive to the value of l/a. This will be discussed later in detail. The reversed position shifts to the outside with an increase of the modulation frequency, i.e., from $r/a \cong 0.5$(30Hz) to $r/a \cong 0.7$(100Hz)

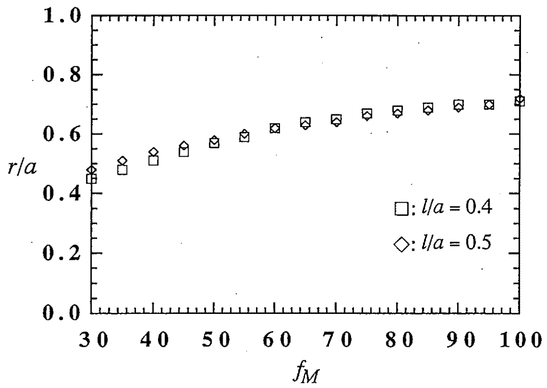

Fig. 4.9 The frequency dependence of the phase reversed position. The points of □ and ◇ are for l/a=0.4 and 0.5, respectively. We set C_{global}=0.1. The reversed phase appears. The position shifts to the outside with the increase of the frequency, f_M.

l/a dependence

The phase reversed position is plotted versus l/a

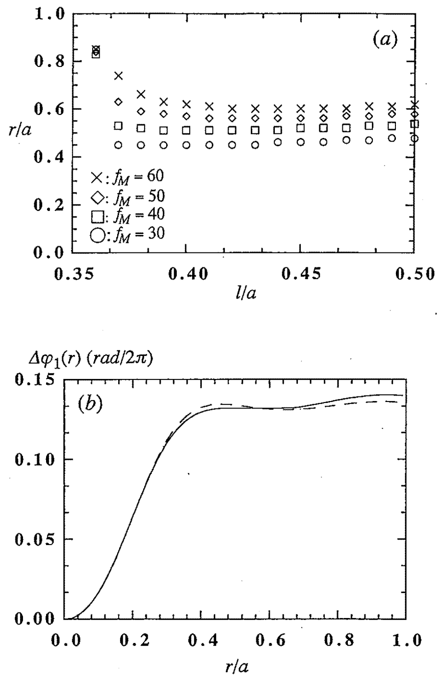

Fig. 4.10 The l/a dependence of the phase reversed position (a). The points of ○, □, ◇ and × are obtained for f_M(Hz)=30, 40, 50 and 60, respectively. We set C_{global}=0.1. There is a critical value of l/a for the appearance of the reversed phase. The radial profiles of the phase difference compared for l/a=0.36 (solid line) and l/a=0.37 (dashed line), respectively, for f_M=30Hz (b). The variation between the radial profile is small compared with the phase reversed position.

in figure 4.10 (a) for f_M=30 (Hz) (○), 40 (□), 50 (◇) and 60 (×), where C_{global} is fixed to 0.1. When l/a is smaller than 0.36, the reversed phase is hardly observed. Above the critical value, the reversed phase suddenly appears. The critical value is seen to be insensitive to the frequency. The position shifts to the outside with the increase of frequency. Although the phase reversed position drastically changes near the critical value of l/a, the difference in the radial profiles of phase difference $\Delta\varphi_1(r)$ is small. The comparison is shown in figure 4.10 (b) between the cases for l/a=0.36 (the solid line) and l/a=0.37 (the dashed line), where f_M and C_{global} are fixed to 30Hz and 0.1, respectively. For l/a=0.36, the profile of $\Delta\varphi_1(r)$ is nearly flat in the outside region and reversed phase does not appear. On the other hand, for l/a=0.37, the local maximum appears in the middle region. Thus, the phase reversed position jumps from the outside to the inside with a small change of l/a (from 0.36 to 0.37). The fact that the reversed phase is observed in the experiment suggests that, if the non-local transport of the form equation (3.5) exists, there exists a fairly large correlation length ($l/a \geq 0.37$ for C_{global}=0.1).

C_{global} dependence

The dependence of the phase reversed position on C_{global} is shown in figure 4.11 for l/a=0.4 (□) and 0.5 (◇), where f_M is fixed to 30Hz. We see that the phase reversed position shifts to the inside with the increase of C_{global} for l/a=0.4 and 0.5. It is hardly seen the difference in the C_{global} dependence between l/a =0.4 and 0.5. Thus, if f_M and C_{global} are fixed to some values and l/a is larger than the critical value, the phase reversed position is not sensitive to the value of l/a.

The contour of the phase reversed position

The contour of the phase reversed position at r/a =0.5 (○), r/a=0.6 (□), and r/a=0.7 (◇) are shown on l/a and C_{global} plane in figure 4.12, where f_M is fixed to 30Hz. The vertical axis is C_{global} and horizontal axis is l/a. It is seen that the phase reversed position shifts to the inside with the increase of C_{global} for fixed l/a, while it slightly depends on l/a. This show dependence of l/a on the phase reversed position indicates that if the phase reversed positions are observed in experiments with the modulation frequency f_M=30Hz, then it may be possible to determine the lowest boundary of C_{global}.

5. Summary and Discussion

In this thesis, a new transport model, in which the non-local effect is taken into account, was discussed. This expression assumes that the heat flux at r is influenced by the temperature gradient far from the location r. Such a situation is expected when the flow is influenced by large scale convections, the scale length of which is comparable to the gradient scale length. The energy transport equation was re-

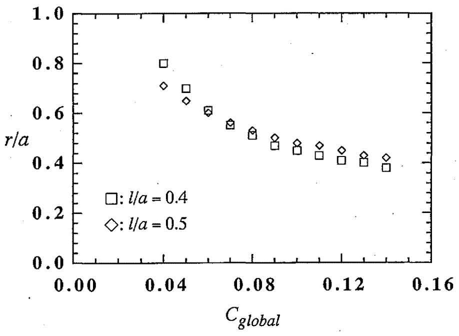

Fig. 4.11 The C_{global} dependence of the phase reversed position. The points of □ and ◇ are obtained for l/a=0.4 and 0.5, respectively. We set f_M=30Hz. The reversed phase appears and the positions shift to the inside with the increase of C_{global}.

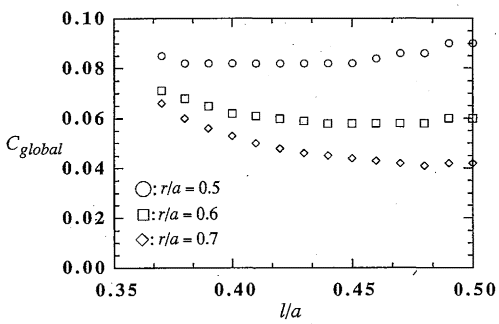

Fig. 4.12 The contour of the phase reversed position. The points of ○, □, ◇ are obtained for r/a=0.5, 0.6, and 0.7, respectively. We set f_M=30Hz. The phase reversed position is more sensitive to C_{global} that to l/a.

formulated into the integro-differential equation.

We simulated the input power switching experiment. Solving the energy transport equation with the assumptions that the electron density and diffusivity are constant, the gradient-flux relation in the transient response was obtained. The hysteresis appears in their dynamic relation. This hysteresis is not obtained in a local transport model in which the coefficient is expressed by local plasma parameters and gradients. The findings in the experiment in W7-AS [9] and of an analysis using a global power dependent ansatz [11] were reproduced by our non-local transport model, which is based on an integral over local plasma parameters. We also investigated the characteristics of the hysteresis with respect to the observation point and the switching time of central heating power, t_c. We obtained the following results, i) On the hysteresis curve the plasma dynamics is seen to follow in the clockwise direction when it is observed at the location far from the power deposition, while it is in the counter-clockwise direction if it is observed at the region heated directly. ii) The peak of the width of the hysteresis is observed at $r/a \approx l/a + r_0$. (for $r > r_0$ and r_0 is close to the ridge of the power deposition region.) If the width of the hysteresis can be measured as a function of radius and if a maximum is observed in such a relation, an information on the correlation length of the non-local effect may be obtained. iii) The hysteresis is prominent when $t_c \ll \tau_E$ and the width decays proportional to $1/t_c$.

We also simulated the power modulation experiment done in W7-AS. The perturbation of temperature was examined with respect to the amplitude and the phase. The difference of the Fourier decomposed phases between the observation point and the center was analyzed. It is found that the peak value of the phase difference appears inside the plasma in the transient response. The reverse of the phase difference is observed in the radial dependence. The obtained reversed phase is considered to correspond to the findings in the experiment. The influence of the boundary effect is also investigated and it is confirmed that the appearance of the reversed phase is not due to the boundary effect but due to the non-local effect. Furthermore, we investigated the dependences of the position of phase reversal on f_M, l/a and C_{global}. Results are as follows, i) The position of phase reversal shifts to the outside with the increase of f_M. ii) There is a critical value of l/a for the appearance of the reversed phase. The critical value is insensitive to the modulation frequency f_M. The radial dependence of the phase difference shows a slight change across the critical value of l/a. The fact that the reversed phase is observed in the experiment suggests that a rather large non-local effect ($l/a \geq 0.37$) may exist in the framework of our analyses. iii) The phase reversed position shifts to the inside with the increase of C_{global}. iv) Finally, the various dependences of the phase reversed position are summarized in figure 4.12. This figure indicates that if the position of phase reversal are analyzed in experiments, it may be possible to determine the lower boundary of C_{global}.

The model proposed in this thesis provides an alternative way to the model in [9, 11] in understanding the transient transport phenomena in W7-AS stellarators. It seems to merit further application of this model to various circumstances in order to fully understand the nature of the non-local transport model. The electron density and diffusivity are assumed to be constant through this simulation. To perform a quantitative test of this new model for the mechanism of the transient transport, the dependence of χ_e on plasma parameters must be incorporated. Study of the radial profile of the density and study of the dependence of the diffusivity on temperature or temperature gradient are left for our future work. In this paper, we assumed that the transport is governed by the Markovian process for simplicity. The transport model which is taken the non-Markovian process into account should be also studied in the future.

Acknowledgment

The author would like to thank Prof. S.-I. Itoh for her guidance, support and continuous encouragement during the course of research, and Dr. M. Yagi for useful comments, suggestions and help with respect to the computer simulations.

Special thanks are also extended to Prof. K. Itoh and Dr. U. Stroth for the creative comments.

Furthermore, the author is grateful to his colleague; Drs. S. Toda, T. Kubota, Messrs. G. Tateishi, N. Yamamoto and T. Fujimoto for fruitful discussion.

Finally, the author wishes to thank his family for their support.

Appendix A

Numerical Algorithm for the Non-local Model and its Convergence Check

In this Appendix, we give a numerical algorithm for the non-local model and do a convergence check of it. The numerical algorithm which is used for solving the integro-differential equation (i.e., equation (3.5)) is explained in detail.

We start from equation (3.5). Variables are normalized as $T/T_0 \to T$, $t/\tau_E \to t$, $r/a \to x$, $l/a \to l$ and $\chi_e \tau_E/a^2 \to \chi_0$, where T_0 is a typical plasma temperature and τ_E is the energy confinement time. Then equation (3.5) is reduced to

$$\frac{\partial T(x,t)}{\partial t}=a\left(\frac{1}{x}\frac{\partial T(x,t)}{\partial x}+\frac{\partial^2 T(x,t)}{\partial x^2}+S(x,t)\right)+P(x,t), \tag{A.1}$$

where

$$a=\frac{2}{3}\chi_0 C_{\mathrm{local}}, \tag{A.2}$$

$$S(x,t)=2\frac{C_{\mathrm{global}}}{C_{\mathrm{local}}}\left\{\int_0^1 \frac{1}{\sqrt{\pi}\,l}\left(1-x\frac{x-x'}{l^2}\right)\frac{1}{x'}\exp\left[-\left(\frac{x-x'}{l}\right)^2\right]\frac{\partial T(x',t)}{\partial x'}dx'\right\}, \tag{A.3}$$

$$P(x,t)=\frac{2\tau_E}{3n_e T_0}\Sigma Q. \tag{A.4}$$

The integration in $S(x,t)$ can be easily performed, for example, by use of the Simpson's rule if the temperature profile is given at one time step before.

Each term in (A.1) is discretised as

$$\frac{\partial T}{\partial t}\to(1+\gamma)M_x\frac{\Delta T_j^{n+1}}{\Delta t}-\gamma M_x\frac{\Delta T_j^n}{\Delta t}, \tag{A.5}$$

$$\frac{1}{x}\frac{\partial T}{\partial x}\to\frac{1}{x_j}\beta L_x T_j^{n+1}+\frac{1}{x_j}(1-\beta)L_x T_j^n, \tag{A.6}$$

$$\frac{\partial^2 T}{\partial x^2}\to\beta L_{xx}T_j^{n+1}+(1-\beta)L_{xx}T_j^n, \tag{A.7}$$

$$S\to S_j^n,\ P\to P_j^n, \tag{A.8}$$

where

$$M_x\Delta T_j\equiv\delta\Delta T_{j-1}+(1-\delta)\Delta T_j+\delta\Delta T_{j+1}, \tag{A.9}$$

$$\Delta T_j^{n+1}\equiv T_j^{n+1}-T_j^n,\ \Delta T_j^n\equiv T_j^n-T_j^{n-1}, \tag{A.10}$$

$$L_x T_j\equiv\frac{T_{j+1}-T_{j-1}}{2\Delta_x}, \tag{A.11}$$

$$L_{xx}T_j\equiv\frac{T_{j+1}-2T_j+T_{j-1}}{\Delta x^2}. \tag{A.12}$$

The subscript j represents the j-th mesh of x and the subscript n represents the n-th time step such as $x_j=j\Delta x$ and $t^n=n\Delta t$, where Δx is the mesh size of x and Δt is the step size of t. The parameters β, γ and δ may be chosen to provide particular levels of accuracy and/or stability. The values of $\delta=0$ and $\delta=1/6$ correspond to the finite difference method and the finite element method, respectively. At the fixed values of $\delta=0$ and $\gamma=0$, the choices of $\beta=0.0$, 0.5, 1.0 give the full explicit method, Crank-Nicolson method and full implicit method, respectively.

Substituting the equations (A.5)-(A.8) into equation (A.1), we obtain

$$A_jT_{j-1}^{n+1}+B_jT_j^{n+1}+C_jT_{j+1}^{n+1}=D_jT_{j-1}^n+E_jT_j^n+F_jT_{j+1}^n+G_jT_{j-1}^{n-1}+H_jT_j^{n-1}+I_jT_{j+1}^{n-1}+J_j, \tag{A.13}$$

where

$$A_j=(1+\gamma)\delta+\left(\frac{\Delta x}{2x_j}-1\right)\beta s, \tag{A.14}$$

$$B_j=(1+\gamma)(1-2\delta)+2\beta S, \tag{A.15}$$

$$C_j=(1+\gamma)\delta-\left(\frac{\Delta x}{2x_j}+1\right)\beta s, \tag{A.16}$$

$$D_j=(1+2\gamma)\delta-\left(\frac{\Delta x}{2x_j}-1\right)(1-\beta)s, \tag{A.17}$$

$$E_j=(1+2\gamma)(1-2\delta)-2(1-\beta)s, \tag{A.18}$$

$$F_j=(1+2\gamma)\delta+\left(\frac{\Delta x}{2x_j}+1\right)(1-\beta)s, \tag{A.19}$$

$$G_j=-\gamma\delta, \tag{A.20}$$

$$H_j=-\gamma(1-2\delta), \tag{A.21}$$

$$I_j=-\gamma\delta, \tag{A.22}$$

$$J_j=\Delta x^2 sS_j^n+\Delta tP_j^n, \tag{A.23}$$

and

$$s=a\frac{\Delta t}{\Delta x^2}. \tag{A.24}$$

Equation (A.13) produces a tridiagonal system of equations at every node. Therefore if appropriate initial condition and boundary conditions are given, equation (A.1) can be solved. In this study, the finite difference and the full implicit method is used, i.e., $\delta=0$, $\gamma=0$ and $\beta=1.0$.

To confirm the convergence of this algorithm, we investigated the dependence of the mesh size Δx on the width of the hysteresis. Figure A.1 shows the width at various values of Δx. Parameters are chosen as the same value used in the section 4.1. For these parameters, the hysteresis is observed at $r/a=0.1$ for $l/a=0.3$. The convergence is fairly good for small value of Δx.

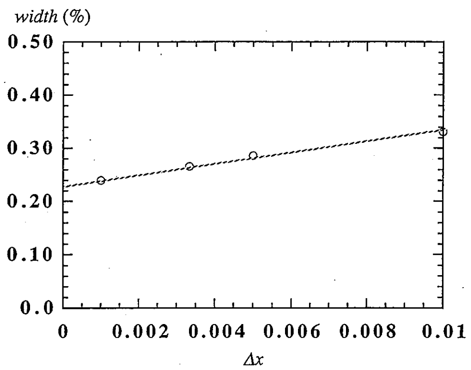

Fig. A1 The width of the hysteresis is plotted at various value of Δx for the convergence check. In this case, the hysteresis is observed at $r/a=0.1$ for $l/a=0.3$. The convergence is fairly good for small value of Δx.

References

[1] Callen J D and Jahns G L 1977 *Phys. Rev. Lett.* **38** 491

[2] Fredrickson E D, Callen J D, McGuire K, et al 1986 *Nucl. Fusion* **26** 849

[3] Lopes Cardozo N J, Tubbing B J D, Tibone F, et al 1988 *Nucl. Fusion* **28** 1173

[4] Lopes Cardozo N J, 1995 *Plasma Phys. Control. Fusion* **37** 799

[5] Callen J D and Kissick M W 1997 *Plasma Phys. Control. Fusion* **39** B173

[6] Neudatchin S V, Cordey J G and Muir D G 1993 *Proc. 20th Eur. Conf. on Controlled Fusion and Plasma Physics (Lisbon)* Europhys. Vol 17C Part I, 83 (Geneva: EPS)

[7] Cordey J G, Muir D G, Neudatchin S V et al 1994 *Plasma Phys. Control. Fusion* **36** A267

[8] Cordey J G, Muir D G, Neudatchin S V, et al 1995 *Nucl. Fusion* **35** 101

[9] Stroth U, Giannone L, Hartfuß H-J, et al 1996 *Plasma Phys. Control. Fusion* **38** 1087

[10] Giannone L, Erckmann V, Gasparino U, et al 992 *Nucl. Fusion* **32** 1985

[11] Stroth U, Giannone L, Hartfuß H-J, et al 1993 Proc. of the Workshop on Local Transport Studies in Fusion Plasma, Varenna 161

[12] Rebut P H, Lallia P P and Watkins M L 1989 *Plasma Physics and Controlled Nuclear Fusion Research (proc. 12th Int. Conf. (Nice, 1988))* Vol 2 (vienna: IAEA) p191

[13] Stroth U 1997 *Plasma Phs, Contr. Fusion* in press

[14] Parail V V, Cherubini A, Cordey J G, et al 1997 *Nucl. Fusion* **37** 481

[15] Kubota T, Iwasaki T, Itoh S-I, et al 1997 *proc. 24 th Eur. Conf. on Controlled Fusion and Plasma Physics (Berchtesgaden)* Europhys. Vol 21A Part IV, 1769 (Geneva: EPS)

[16] Ejima S, Okabayashi M and Schmidt J 1974 *Phys. Rev. Lett* **32** 872

[17] Jahns G L, Soler M, Waddell B V, et al 1978 *Nucl. Fusion* **18** 609

[18] Lopes Cardozo N j, Konings J A and Peters M 1992 *Nucl. Fusion* **32** 1671

[19] Wagner F and Stroth U 1993 *Plasma Phys. Control. Fusion* **35** 1321

[20] Tubbing B J D, Lopes Carcozo N J and Van der Wiel M J 1987 *Nucl. Fusion* **27** 1843

[21] Gentle K W 1988 *Phys. Fluids* **31** 1105

[22] Fredrickson E D, McGuire K, Cavallo A, et all 1990 *Phys. Rev. Lett* **65** 2869

[23] Lopes Cardozo N J and Sips A C C 1991 *Plasma Phys. Control. Fusion* **33** 1337

[24] Takase Y, Goldston R J, Bell M G, et al 1992 *Nucl. Fusion* **32** 2246

[25] Yamaguchi H 1995 *Master Thesis,* in Kyushu University; Yamaguchi H and Itoh S-I 1995 *J. Phys, Soc. Jpn* **64** 1051

[26] Cordey J G, Muir D G,Parail V V, et al 1995 *Nucl. Fusion* **35** 505

[27] Kissick M W, Fredrickson E D, Callen J D, et al 1994 *Nucl. Fusion* **34** 349

[28] Gentle K W, Bravenec R V, Cima G, et al 1995 *Phys. Plasmas* **2** 2292

[29] JET TEAM 1995 *Plasma Physics and Controlled Nuclear Fusion Research* (*Proc. 15th Int. Conf.* (*Seville, 1994*)) Vol 1 (Vienna: IAEA) p307

[30] Giannone L, Stroth U, Köllermeyer, et al 1996 *Plasma Phys. Control. Fusion* **38** 477

[31] Lopes Cardozo N J, de Haas J C M, Hogeweij G M D, et al *Plasma Phys. Control. Fusion* **32** 983

[32] Itoh K, Itoh S-I, Fukuyama A, et al 1994 *Plasma Phys. Control. Fusion* **36** 279

[33] See, e.g, Luce T, Petty C C, Burrell K H, et al 1995 *Plasma Physics and Controlled Nuclear Fusion Research* (*Proc. 15the Int. Conf.* (*Seville, 1994*)) Vol 1 (Vienna: IAEA) p319

[34] Connor J W and Taylor J B 1977 *Nucl. Fusion* **17** 1047

[35] Peters M 1995 *Doctoral Thesis,* in Technische Universiteit Eindhoven